Research Square

Preprints are preliminary reports that have not undergone peer review.
They should not be considered conclusive, used to inform clinical practice,
or referenced by the media as validated information.

Engineering ArtE2, a polycationic peptide-fused Bacillus endolysin, expands antibacterial activity to Escherichia coli while retaining potency against Staphylococcus aureus

Roxana Portieles
Joint R&D Center of Biotechnology, RETDA, Yota Bio-engineering Co., Ltd.
Xinmin Ma
Joint R&D Center of Biotechnology, RETDA, Yota Bio-engineering Co., Ltd.
Jianjian Hu
Joint R&D Center of Biotechnology, RETDA, Yota Bio-engineering Co., Ltd.
Yuxiu Xu
Joint R&D Center of Biotechnology, RETDA, Yota Bio-engineering Co., Ltd.
Hongli Xu
Joint R&D Center of Biotechnology, RETDA, Yota Bio-engineering Co., Ltd.
Wang Ling
Joint R&D Center of Biotechnology, RETDA, Yota Bio-engineering Co., Ltd.
Xiangyou Gao
Joint R&D Center of Biotechnology, RETDA, Yota Bio-engineering Co., Ltd.
Nayanci Portal-González
School of Biological Science and Technology, University of Jinan
Rabia Durrani
National Key Laboratory for Development and Utilization of Forest Food Resources, Zhejiang A&F University
Ramón Santos-Bermúdez
School of Biological Science and Technology, University of Jinan
Orlando Borras-Hidalgo
oborrash2023@qq.com

Joint R&D Center of Biotechnology, RETDA, Yota Bio-engineering Co., Ltd.

Research Article

Keywords: Artilysin, Endolysin engineering, Antibacterial protein, Bacillus altitudinis, Escherichia coli, Staphylococcus aureus, Peptidoglycan, Molecular docking

Posted Date: November 5th, 2026

DOI: https://doi.org/10.21203/rs.3.rs-10886723/v1

License: This work is licensed under a Creative Commons Attribution 4.0 International License.
Read Full License

Additional Declarations: No competing interests reported.

Engineering ArtE2, a polycationic peptide-fused Bacillus endolysin, expands antibacterial activity to Escherichia coli while retaining potency against Staphylococcus aureus

Roxana Portieles[1], Xinmin Ma[1], Jianjian Hu[1], Yuxiu Xu[1], Hongli Xu[1], Wang Ling[1], Xiangyou Gao[1], Nayanci Portal-González[2], Rabia Durrani[3,4], Ramón Santos-Bermúdez[2,*], Orlando Borrás-Hidalgo[1,5*]

1 Joint R&D Center of Biotechnology, RETDA, Yota Bio-engineering Co., Ltd., 99 Shenzhen Road, Rizhao 276826, Shandong, People's Republic of China.

2 School of Biological Science and Technology, University of Jinan, No. 336, West Road of Nan Xinzhuang, Jinan 250022, Shandong, People's Republic of China.

3 National Key Laboratory for Development and Utilization of Forest Food Resources, Zhejiang A&F University, Hangzhou 311300, People's Republic of China.

4 Provincial Key Laboratory for Non-wood Forest and Quality Control and Utilization of Its Products, Zhejiang A&F University, Hangzhou 311300, People's Republic of China.

5 College of Agriculture and Biology, Liaocheng University, 1 Hunan Road, Liaocheng 252000, Shandong, People's Republic of China.

**Correspondence: Orlando Borrás-Hidalgo (oborrash2023@qq.com); Ramón Santos-Bermúdez (bio_ramon@ujn.edu.cn)*

Abstract

Background: The outer membrane of Gram-negative bacteria restricts access of most exogenously applied endolysins to peptidoglycan. This study aimed to engineer ArtE2 from Bacillus altitudinis Endolysin-2 (E2) by fusing the polycationic decapeptide MKRKKRKKRK to the N-terminus and introducing the substitutions H176Y and T178R, and to evaluate its antibacterial activity against Escherichia coli while determining whether activity against Staphylococcus aureus was retained.

Results: ArtE2 was obtained as a soluble, highly cationic protein. Molecular docking predicted interactions with several peptidoglycan fragments, including the NAG–NAM dimer. ArtE2 displayed concentration- and time-dependent antibacterial activity against both E. coli ATCC 25922 and S. aureus ATCC 25923, whereas native E2 showed little activity against E. coli. Measurable residual activity was retained across the temperature and pH ranges examined. Molecular dynamics simulations revealed condition-dependent differences in RMSD, with comparatively low values under selected conditions, including pH 7 in the presence of $CaCl_2$.

Conclusions: ArtE2 showed enhanced antibacterial activity relative to native E2 against the strains tested. Evaluation against a broader and more clinically diverse bacterial panel is warranted.

Keywords: Artilysin; Endolysin engineering; Antibacterial protein; Bacillus altitudinis; Escherichia coli; Staphylococcus aureus; Peptidoglycan; Molecular docking

Background

Antimicrobial resistance (AMR) remains a major global health challenge. Its emergence can be driven by multiple selective pressures, including exposure to certain non-antibiotic drugs [1]. The 2024 World Health Organization (WHO) Bacterial Priority Pathogens List classifies third-generation cephalosporin-resistant and carbapenem-resistant Enterobacterales, including resistant Escherichia coli and Klebsiella pneumoniae, as critical-priority pathogens [2]. The substantial global burden of bacterial AMR highlights the need for antibacterial agents with novel mechanisms of action [3].

Bacteriophage-derived endolysins have emerged as promising alternatives to conventional antibacterial agents. These peptidoglycan (PG) hydrolases degrade the bacterial cell wall during the phage lytic cycle [4,5]. When applied exogenously, endolysins can display rapid, species- or genus-specific bactericidal activity, particularly against Gram-positive bacteria [4,5]. However, the outer membrane (OM) of Gram-negative bacteria constitutes a major permeability barrier that prevents most native endolysins from reaching their PG substrate [6].

Protein engineering has produced Artilysins chimeric endolysins fused to cationic or amphipathic peptides that facilitate access to the PG layer by destabilising the OM [6,7]. Briers et al. demonstrated that fusion of a polycationic nonapeptide to selected endolysins conferred antibacterial activity against multidrug-resistant Pseudomonas aeruginosa and Acinetobacter baumannii [6]. Subsequent studies have explored peptide composition, linker design, fusion orientation and related strategies to improve activity against Gram-negative bacteria [7–12].

Bacteriophages that infect Bacillus species encode endolysins with diverse architectures. Many possess a modular organisation comprising an N-terminal enzymatically active domain and a C-terminal cell-wall-binding domain [13]. Several Bacillus-targeting endolysins exhibit rapid exogenous lytic activity against Gram-positive bacteria and have therefore been investigated as potential antibacterial agents [13,14].

In our previous study, Endolysin-2 (E2), a putative phage-derived endolysin identified from Bacillus altitudinis/Bacillus aryabhattai genome resources, was predicted to contain an N-terminal N-acetylmuramoyl-L-alanine amidase domain and a C-terminal SPOR-family cell-wall-binding domain. Among seven native endolysins evaluated, E2 showed the strongest antibacterial activity against the Gram-positive species Staphylococcus aureus and Micrococcus

luteus [15]. Building on these findings, the present study engineered E2 to determine whether its antibacterial spectrum could be extended to the Gram-negative bacterium E. coli while retaining activity against S. aureus. The resulting protein, ArtE2, differs from native E2 by the addition of an N-terminal polycationic decapeptide and the introduction of the substitutions H176Y and T178R. We compared ArtE2 with native E2 in antibacterial assays and evaluated its physicochemical characteristics, predicted interactions with peptidoglycan fragments, and stability under different temperature, pH and ionic conditions.

Methods

Bacterial strains and culture conditions

E. coli ATCC 25922 and S. aureus ATCC 25923 were used as representative Gram-negative and Gram-positive test strains, respectively. The E2 coding sequence was obtained from the B. altitudinis/B. aryabhattai genome resources available under NCBI BioProject PRJNA781678 [15]. E. coli BL21(DE3) was used for recombinant protein expression. Unless otherwise stated, bacterial strains were cultured in Luria–Bertani (LB) broth or on LB agar at 37 °C. E. coli BL21(DE3) harbouring expression constructs was grown in LB broth supplemented with ampicillin (100 μg mL^{-1}).

Gene cloning and construction of the ArtE2 expression vector

The E2 coding sequence was amplified with primers Endolysin 2 F and Endolysin 2 R, while ArtE2 was generated with primers ArtE2 F and ArtE2 R (Table 1). ArtE2 contains the N-terminal polycationic decapeptide MKRKKRKKRK together with the substitutions H176Y and

T178R. Verified expression constructs encoding ArtE2 and native E2 were introduced into E. coli BL21(DE3) for recombinant protein production.

Recombinant expression and purification of ArtE2

The coding sequences of E2 and ArtE2 (Supplementary Table 1) were amplified by PCR and cloned into the cold-shock expression vector pCold I to generate N-terminal His-tagged constructs. Recombinant plasmids were propagated in E. coli DH5α, verified by Sanger sequencing and transformed into E. coli BL21(DE3). Cultures were grown in LB medium containing ampicillin (100 μg mL^{-1}) at 37 °C to an OD_{600} of approximately 0.6, induced with IPTG (0.5 mM) and expressed at 15–16 °C for 18 h. Cells were harvested by centrifugation and lysed by sonication in binding buffer (20 mM sodium phosphate, 0.5 M NaCl, 30 mM imidazole, pH 7.4). Clarified lysates (centrifugation followed by 0.22 μm filtration) were purified by immobilised metal-affinity chromatography on Ni-NTA resin (HisPur™ Ni-NTA Gravity Column; Thermo Fisher Scientific) according to the manufacturer's instructions. Protein purity was assessed by SDS-PAGE and densitometric analysis; concentrations were determined with the bicinchoninic acid (BCA) assay. Protein concentrations were normalised on a molar basis using theoretical molecular weights calculated from the sequences. Western blotting was performed to confirm the presence of ArtE2. Proteins were resolved by SDS-PAGE, transferred to a polyvinylidene fluoride (PVDF) membrane and blocked for 1 h with 5% (w/v) skimmed milk in PBS. Membranes were incubated overnight at 4 °C with a 1:1000 dilution of mouse anti-6×His primary antibody, washed three times with TBST, and then incubated for 1 h at room temperature with a 1:10 000 dilution of goat anti-mouse HRP-conjugated secondary antibody. Signals were developed with Western Bright ECL reagent and captured on a ChemiDoc MP Imaging System.

Sequence-based physicochemical analyses

Physicochemical properties of ArtE2 were calculated with the Protein Analysis module of Biopython (version 1.87). Parameters included sequence length, molecular weight, theoretical isoelectric point, net charge at pH 7.0, instability index, aliphatic index, grand average of hydropathicity (GRAVY), molar extinction coefficient, aromaticity and predicted secondary-structure fractions. The N-terminal peptide (residues 1–10) was analysed separately from the ArtE2 core (residues 11–261). Kyte–Doolittle hydropathy and Vihinen flexibility profiles were computed using a nine-residue sliding window.

Molecular docking analysis

A three-dimensional model of ArtE2 was generated with AlphaFold2 [25]. Model confidence was assessed using the predicted Local Distance Difference Test (pLDDT). The structure was prepared for docking by removal of water molecules, addition of polar hydrogen atoms and assignment of Gasteiger charges with AutoDockTools (version 1.5.7). Structures of the PG-derived ligands were obtained from PubChem or the Carbohydrate Structure Database (identifiers listed in Table 4). Ligands were prepared with Open Babel (version 3.1.1) and protonated at pH 7.4. Potential ligand-binding pockets were predicted with PrankWeb. Molecular docking was performed with AutoDock Vina (version 1.2.5) [16,17]. The search box was centred on the geometric centre of the highest-scoring predicted pocket (Pocket 1) and set to 25 × 25 × 25 Å. Exhaustiveness was set to 32; ten independent docking runs were performed for each ligand, yielding 20 poses per run. Poses were ranked by Vina score and the highest-ranked pose was selected for interaction analysis. Protein–ligand interactions were visualised in PyMOL (version 2.5.0). Native E2 was analysed using the identical preparation and docking protocol.

Time-kill and concentration-dependent antibacterial assays

Overnight cultures of E. coli ATCC 25922 and S. aureus ATCC 25923 were diluted in fresh LB medium and grown at 37 °C to an OD_{600} of approximately 0.8. Cells were harvested and adjusted to approximately 1×10^8 CFU mL^{-1} in 20 mM HEPES, 50 mM NaCl, pH 7. Bacterial suspensions were mixed with ArtE2 or native E2 to final protein concentrations of 2, 5, 8 or 10 μg mL^{-1} in a total volume of 100 μL. A buffer-only control served as the negative control. Reaction mixtures were incubated at 30 °C under static conditions for 1 h. Samples were withdrawn at 0, 15, 30, 45 and 60 min, serially diluted in sterile phosphate-buffered saline (PBS) and plated (100 μL) onto LB agar. Colonies were counted after 24 h at 37 °C. Viable counts were expressed as $\log_{10}$ CFU mL^{-1}. Where indicated, antibacterial activity was calculated as $\log_{10}(N_control) - \log_{10}(N_treatment)$. The detection limit of the assay was 100 CFU mL^{-1}. Experiments comprised three independent biological replicates, each measured in three technical replicates.

Effects of pre-incubation temperature and pH on ArtE2 activity

To assess the effect of temperature, ArtE2 (5 μg mL^{-1}) was pre-incubated for 30 min at 4, 25, 37, 42 or 56 °C. Samples were returned to 25 °C and residual lytic activity against E. coli ATCC 25922 and S. aureus ATCC 25923 was measured using an optical-density-based lysis assay. Changes in optical density at 600 nm (ΔOD_{600}) were recorded over 30 min. To assess the effect of pH, ArtE2 was incubated for 30 min at 25 °C in 20 mM sodium acetate (pH 4.0–5.5), 20 mM sodium phosphate (pH 6.0–8.0) or 20 mM Tris-HCl (pH 8.5–10.0). After pre-incubation, samples were diluted ten-fold into 10 mM HEPES (pH 7.4) to neutralise the pH, and residual activity was measured with the same ΔOD_{600} assay. ArtE2 maintained under standard conditions

(25 °C in 10 mM HEPES, pH 7.4) served as the reference control. Experiments comprised three independent biological replicates.

Molecular dynamics simulations

The highest-ranked ArtE2–NAG–NAM docking pose was used as the starting structure for molecular dynamics (MD) simulations. Systems were neutralised and supplemented with $CaCl_2$, KCl, $MgCl_2$ or NaCl at 150 mM at either pH 5 or pH 7. Three independent production runs of 1000 ns were performed. Each replica was initiated from the same energy-minimised and equilibrated structure but with different initial velocity distributions generated from distinct random seeds. Simulations were conducted in GROMACS [26] with the CHARMM36m force field [27]. Full-length ArtE2–NAG–NAM complexes were solvated in a cubic TIP3P water box and neutralised with counter-ions. Energy minimisation (5000 steps) was followed by equilibration in the NVT (100 ps, 300 K) and NPT (100 ps, 1 bar) ensembles. Production runs used a 2 fs time step, periodic boundary conditions and particle-mesh Ewald electrostatics. RMSD values were calculated for protein backbone atoms relative to the initial frame of each replica. Structural stability was assessed as the mean RMSD ± standard deviation across the three independent replicas.

Statistical analysis

All experiments were performed in triplicate unless otherwise stated. Data are presented as mean ± standard deviation. One-way ANOVA was used to assess the significance of treatments; differences were considered highly significant at $P < 0.0001$. Analyses were performed with GraphPad Prism (La Jolla, CA, USA).

Results

Design, sequence features and predicted domain architecture of ArtE2

The parental E2 sequence contains a predicted N-acetylmuramoyl-L-alanine amidase domain and a C-terminal SPOR-like cell-wall-binding domain (Figure 1). ArtE2 comprises the E2 sequence fused to the polycationic decapeptide MKRKKRKKRK, together with the substitutions H176Y and T178R. The positions of these modifications are indicated in the sequence alignment shown in Figure 1. The complete insert and cloning junctions were verified by Sanger sequencing.

Sequence-based physicochemical properties of ArtE2

ArtE2 comprises 261 amino acids and has a calculated molecular weight of 28.46 kDa. The protein has a theoretical isoelectric point of 9.87 and a net charge of +13.04 at pH 7.0. Its instability index of 33.6 classifies it as computationally stable, while the aliphatic index is 85.3. The GRAVY value of −0.274 indicates an overall hydrophilic character. The calculated molar extinction coefficient is 15 930 M^{-1} cm^{-1} and the aromaticity is 0.080. Predicted secondary-structure fractions are approximately 34.9% α-helix, 27.2% turn and 34.1% β-sheet (Table 2).

Separate analysis of the two regions of ArtE2 showed that the N-terminal peptide carries a calculated charge of +8.49 at pH 7.0, a theoretical pI of 12.0 and a GRAVY value of −3.500. The ArtE2 core has a calculated charge of +4.28, a theoretical pI of 9.20 and a GRAVY value of −0.145 (Table 3). Thus, the engineered N-terminal peptide accounts for a substantial proportion of the overall positive charge and hydrophilicity of ArtE2. Residue-level flexibility and hydropathy profiles are shown in Figures 2c and 2d, respectively.

Predicted docking of ArtE2 with peptidoglycan fragments

Molecular docking predicted complexes between ArtE2, and all nine peptidoglycan-derived ligands examined (Table 4). The most negative Vina score was obtained for the NAG–NAM dimer (−6.569 kcal mol^{-1}), followed by the NAM pentapeptide (−6.499 kcal mol^{-1}), NAM–L-alanine (−6.322 kcal mol^{-1}), muramyl dipeptide (−6.228 kcal mol^{-1}) and the peptidoglycan monomer (−6.049 kcal mol^{-1}). Less negative scores were recorded for NAM (−5.849 kcal mol^{-1}), muramyl pentapeptide (−5.433 kcal mol^{-1}), pentaglycine (−5.050 kcal mol^{-1}) and NAG (−4.892 kcal mol^{-1}).

For the ArtE2–NAG–NAM complex the top-ranked docking pose lay within a PrankWeb-predicted pocket (score 32.98, probability 0.932, 25 constituent residues, average conservation score 2.769) (Figure 3). Predicted contacts involved Ala17, Ser77, His79, Asn81, Asn126 and Val129. Under the same docking protocol, native E2 yielded a top-ranked NAG–NAM score of −6.002 kcal mol^{-1} (Figure S1). These docking scores are computational rankings and should not be interpreted as experimentally measured binding free energies.

Recombinant expression and purification of ArtE2

ArtE2 was predominantly recovered in the soluble fraction of induced E. coli BL21(DE3) cultures (Figure 4a). After nickel-affinity chromatography the purified preparation contained a predominant band of approximately 28 kDa, consistent with the calculated molecular mass of ArtE2. Densitometric analysis estimated purity at >90%. Native E2 was expressed and purified by the same procedure for comparative antibacterial assays. The approximately 28 kDa His-tagged ArtE2 band was detected by anti-His immunoblotting (Figure 4b).

Antibacterial activity of ArtE2 against E. coli and S. aureus

ArtE2 exhibited antibacterial activity against both E. coli ATCC 25922 and S. aureus ATCC 25923 after 60 min of exposure (Figure 5). Against E. coli, native E2 produced no statistically significant difference relative to the buffer control, whereas ArtE2 reduced viable counts by more than 6 $\log_{10}$ CFU mL^{-1}. Against S. aureus both native E2 and ArtE2 reduced viable counts relative to the buffer control, with lower residual counts observed after ArtE2 treatment (Figure 5).

ArtE2 activity was dependent on both protein concentration and exposure time (Figure 6). Increasing the ArtE2 concentration from 2 to 10 μg mL^{-1} produced a progressive reduction in viable counts for both bacterial species. At 8 and 10 μg mL^{-1} the lowest viable counts were recorded after 60 min; lower concentrations yielded partial reductions, particularly at earlier sampling times (Figure 6).

Effects of pre-incubation temperature and pH on residual ArtE2 activity

ArtE2 retained measurable residual lytic activity across the temperature and pH conditions examined (Figure 7). The highest ΔOD_{600} values were observed after exposure at 37 °C for both S. aureus and E. coli (Figure 7a). Activity declined at temperatures above or below 37 °C, reaching the lowest values at 56 °C. In the pH series the highest residual activity against S. aureus was recorded at pH 6, whereas the highest activity against E. coli occurred at pH 7 (Figure 7b). Activity decreased under more acidic and more alkaline conditions. These results indicate that ArtE2 activity was greatest at 37 °C and near-neutral pH under the assay conditions used.

Molecular dynamics simulations under different pH and ionic conditions

Backbone RMSD of the predicted ArtE2–NAG–NAM complex varied across the simulated pH and ionic conditions (Figure 8a). Relatively low RMSD values were observed in the system simulated at pH 7 with $CaCl_2$, whereas higher values were recorded under certain alternative conditions. In antibacterial assays performed under corresponding ionic conditions, ArtE2 at pH 7 with $CaCl_2$ produced lower residual viable counts than ArtE2 at pH 7 with $MgCl_2$ against both E. coli (Figure 8b) and S. aureus (Figure 8c). These parallel observations are consistent with a possible association between the simulated behaviour of the complex and ArtE2 activity under the conditions tested.

Discussion

This study provides proof-of-concept evidence that engineering of native E2 can extend its antibacterial activity to a Gram-negative test strain while preserving activity against a Gram-positive target. Native E2 was previously identified as the most active of seven putative Bacillus-associated endolysins evaluated against S. aureus and M. luteus [15]. Here, ArtE2 displayed concentration- and time-dependent activity against E. coli ATCC 25922, whereas native E2 showed little activity under identical conditions. ArtE2 also retained activity against S. aureus ATCC 25923. These findings distinguish the present work from the earlier characterisation of native E2 and identify ArtE2 as a candidate for broader antibacterial evaluation.

ArtE2 combines the polycationic peptide MKRKKRKKRK with the substitutions H176Y and T178R. The fusion peptide increases the calculated positive charge of the engineered N-terminal region a property consistent with established strategies for enhancing endolysin activity against Gram-negative bacteria. Polycationic, amphipathic and membrane-active peptides have been fused to a range of endolysins to promote interaction with the negatively charged bacterial

surface and thereby improve access to peptidoglycan [6,20,21]. The performance of such constructs depends on the parental enzyme, peptide sequence, fusion orientation, linker architecture, charge distribution and assay environment [20,21]. ArtE2 extends this engineering framework to E2, an amidase that contains a predicted SPOR-family cell-wall-binding domain. The present experiments, however, did not directly assess outer-membrane binding or permeabilisation; increased access to peptidoglycan therefore remains a plausible working hypothesis rather than a demonstrated mechanism.

At 10 μg mL^{-1}, ArtE2 produced a >6-log_{10} reduction in viable E. coli ATCC 25922 counts after 60 min. Under the same conditions ArtE2 also markedly reduced viable S. aureus ATCC 25923 counts. The concentration- and time-dependent responses observed against both strains support a treatment-dependent antibacterial effect. This behaviour is qualitatively consistent with that of other peptide-fused endolysins, including Art-175, LysECD7-SMAP, cecropin A-fused LNT113 and cell-penetrating-peptide-fused constructs targeting Gram-negative bacteria [7,8,18,22–24]. Such comparisons support the broader engineering rationale but should not be taken as evidence that ArtE2 is more potent, because the studies differ in bacterial species and strains, starting inocula, protein concentrations, buffers, exposure periods and assay endpoints.

The substitutions H176Y and T178R were identified by comparative sequence analysis as candidates for modifying interactions with peptidoglycan. Docking predicted poses for ArtE2 with several peptidoglycan-derived fragments, the NAG–NAM dimer yielding the most negative Vina score. For the same ligand the top-ranked pose of native E2 was less favourable under the identical docking protocol. This difference offers a structural hypothesis for further investigation, although it cannot establish improved substrate affinity or catalytic activity. Vina scores are approximate ranking functions rather than experimental binding affinities or rigorous free-energy

estimates [16,17]. Because the fusion peptide and both substitutions were introduced together, the present findings reflect the overall performance of the combined ArtE2 design. The observed activity may therefore arise from cooperative contributions of these engineering elements—an interpretation that can be tested in future structure–function studies using modification-specific constructs.

ArtE2 retained measurable residual lytic activity after short-term exposure to the temperature and pH ranges tested, providing an initial indication of physicochemical robustness. Molecular dynamics simulations likewise identified condition-dependent differences in backbone RMSD, with comparatively low values in selected systems, including the pH 7 / $CaCl_2$ condition. Greater antibacterial activity was observed under the corresponding experimental condition. This qualitative concordance suggests that pH and ionic composition may be relevant variables for future optimisation. It does not, however, demonstrate a causal relationship between backbone RMSD and antibacterial activity, because backbone RMSD is not a direct measure of ligand retention, substrate affinity or catalytic efficiency. In addition, Ca^{2+} may influence several components of the assay environment [19], including the bacterial envelope and protein–substrate interactions; these possibilities were not distinguished in the present study.

Taken together, the experimental and computational findings support ArtE2 as a promising engineered derivative of E2 and generate testable structural hypotheses for further characterisation. Evaluation across a broader range of bacterial strains including clinical and multidrug-resistant isolates and experimental settings will be required to determine the breadth, robustness and potential applications of its antibacterial activity. Direct assays of outer-membrane permeabilisation and the construction of intermediate variants (peptide-only and mutation-only) would further clarify the contribution of each engineering element.

Conclusions

ArtE2, an engineered derivative of E2 that contains an N-terminal polycationic peptide and the substitutions H176Y and T178R, exhibited enhanced antibacterial activity against E. coli ATCC 25922 relative to native E2 while retaining activity against S. aureus ATCC 25923. Sequence-based analyses predicted a high net positive charge. Molecular docking and molecular dynamics simulations generated hypotheses concerning interactions with peptidoglycan fragments and conformational behaviour under varying pH and ionic conditions. These computational findings do not establish improved substrate affinity, nor do they explain the experimentally observed antibacterial activity. Because the study was limited to two antibiotic-susceptible reference strains and did not resolve the individual contributions of the peptide and the amino-acid substitutions, neither broad-spectrum activity nor the underlying mechanism can yet be claimed. Overall, the findings support further evaluation of ArtE2 against a broader and more clinically diverse panel of bacteria.

Declarations

Ethics approval and consent to participate

Not applicable.

Consent for publication

Not applicable.

Availability of data and materials

All data supporting the reported results are contained within the article and its supplementary materials. The nucleotide sequence of the ArtE2 construct generated in this study has been deposited in the GenBank repository under accession number PZ766580. The datasets generated and/or analyzed during the current study are available from the corresponding author on reasonable request.

Competing interests

The authors declare that they have no competing interests.

Funding

This study was supported by the Special Funds for Guiding Local Science and Technology Development of the Central Government of Shandong Province (No. YDZX20193700004362).

Authors' contributions

O.B.-H., R.S.-B. and R.P. designed the study, performed the bioinformatics analysis and wrote the manuscript. R.P., X.M., J.H., Y.X., H.X., W.L., X.G., N.P.-G., R.D., R.S.-B. and O.B.-H. performed the experiments. R.P., X.M., J.H. and Y.X. assisted with endolysin purification. O.B.-H., R.P., R.S.-B. and N.P.-G. contributed to data analysis. All authors read and approved the final manuscript.

Acknowledgements

The authors thank the technical staff at the Joint R&D Center of Biotechnology (Yota Bio-Engineering) and the College of Agriculture and Biology (Liaocheng University) for assistance

with protein production and bioassays. Computational resources provided for molecular docking and MD simulations are gratefully acknowledged.

Tables

Table 1. Primer sequences used for amplification of endolysin genes.

Gene Name	Forward Primer (5′–3′)	Reverse Primer (5′–3′)
Endolysin 2	GCATCTAGAATGGTGAAAATTTTTATTGATC	TTATCTAGATTATTGAAAAACGAATGCGTCG
ArtE2	GGTCGGAATTCCATATGAAACGCAAGAAAC	GGTTGGGGATCCTTACTGAAACACGAAC

Forward and reverse primers (5'–3') used to amplify the coding regions of the native endolysin and the engineered ArtE2 construct.

Table 2. Key physicochemical properties of ArtE2 calculated with Biopython Protein Analysis (v1.87).

Parameter	Value	Interpretation / Note
Sequence length	261 aa	—
Molecular weight	28.46 kDa	Suitable for recombinant production
Theoretical isoelectric point (pI)	9.87	Strongly basic
Net charge at pH 7.0	+13.04	Highly cationic – favours interaction with the OM
Instability index	33.6	< 40 → predicted to be stable in vitro
Aliphatic index	85.3	Favourable indicator of thermostability
GRAVY (Kyte–Doolittle)	−0.274	Overall hydrophilic character
Molar extinction coefficient (280 nm)	15 930 M^{-1} cm^{-1}	Reduced form; used for A_{280} quantification
Aromaticity	0.080	Low (fraction of F + W + Y)
Secondary structure (helix / turn / sheet)	~34.9% / 27.2% / 34.1%	Mixed fold typical of endolysins

Table 3. Comparative physicochemical analysis of the N-terminal polycationic peptide and the E2 core.

Property	N-terminal Peptide (1–10)	E2 Core (11–261)
Length	10 aa	251 aa
Net charge (pH 7)	+8.49	+4.28
Theoretical pI	12.00	9.20
GRAVY	−3.500	−0.145
Instability index	106.8	31.0
Principal functional role	Membrane interaction and electrostatic targeting	Catalytic activity and PG binding

Physicochemical properties of the engineered N-terminal polycationic decapeptide (MKRKKRKKRK) compared with those of the E2 endolysin core (residues 11–261).

Table 4. Docking scores of ArtE2 with peptidoglycan fragments ordered by predicted binding affinity.

Rank	Ligand / PG Fragment	Identifier	ΔG (kcal mol^{-1})
1	NAG–NAM dimer	PubChem CID 72210857	**−6.569**
2	NAM-L-Ala-γ-D-Glu-L-Lys-D-Ala-D-Ala (NAM-pentapeptide stem)	CC-DPS CT1103206303	−6.499
3	NAM–L-alanine	PubChem CID 10970945	−6.322
4	NAM-L-alanyl-D-isoglutamine (muramyl dipeptide)	PubChem CID 451714	−6.228
5	Peptidoglycan monomer (NAG–NAM + stem peptide)	CC-DPS CT1079218991	−6.049
6	N-acetylmuramic acid (NAM)	PubChem CID 5462244	−5.849
7	Muramyl pentapeptide	CC-DPS CT1080279170	−5.433
8	Pentaglycine (cross-bridge peptide)	PubChem CID 81537	−5.050
9	N-acetylglucosamine (NAG)	PubChem CID 24139	−4.892

ΔG values are given in kcal mol⁻¹; more negative numbers indicate stronger predicted binding. These are computational ranking scores and should not be interpreted as experimental binding free energies.

Figures

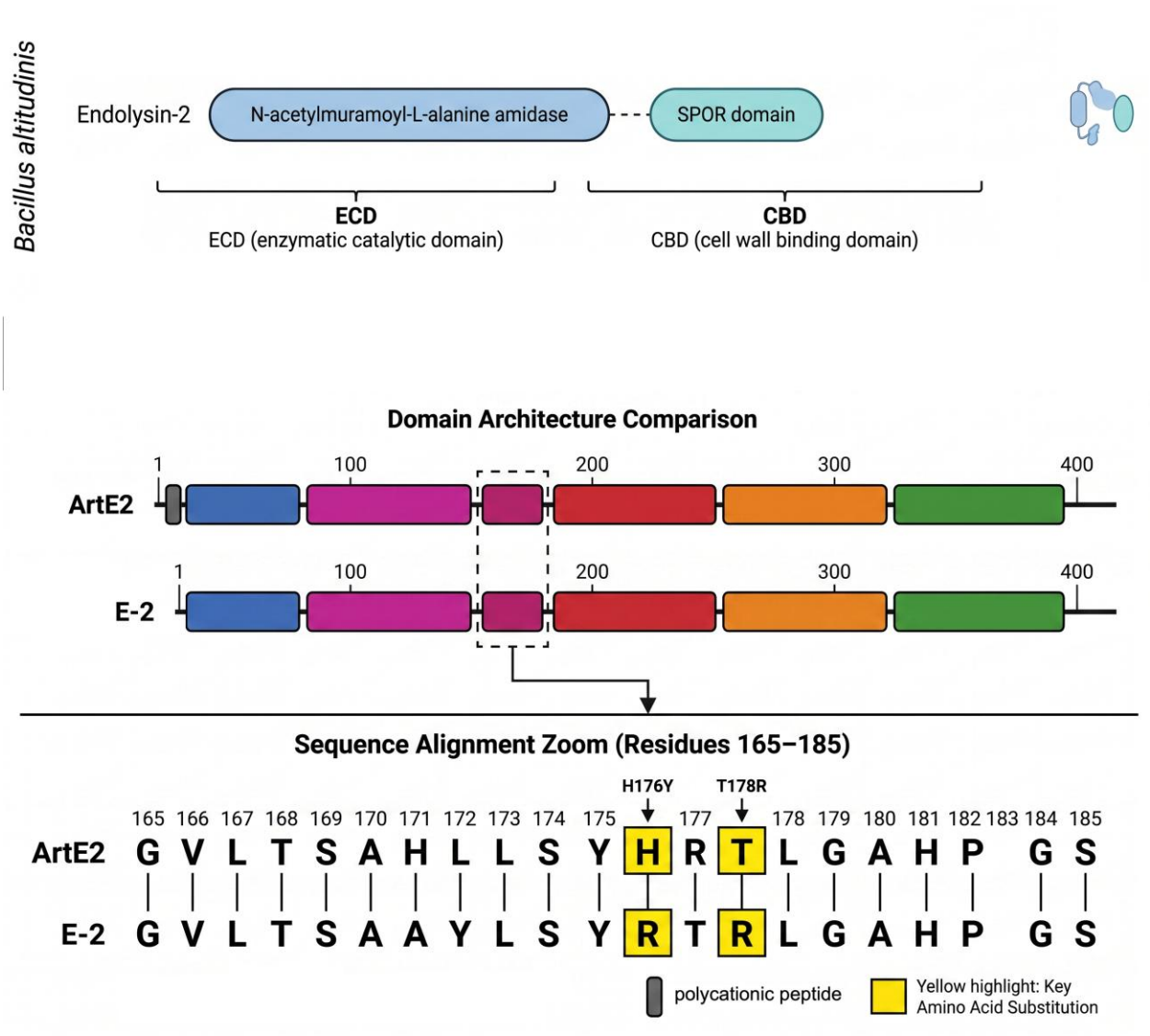


Figure 1. Sequence alignment and domain-architecture comparison between ArtE2 and native E2. Top: domain organisation of Endolysin-2 showing the N-acetylmuramoyl-L-alanine amidase (ECD) and SPOR-like cell-wall-binding domain (CBD). Middle: schematic comparison of ArtE2 (with N-terminal polycationic peptide) and E2. Bottom: sequence alignment zoom (residues 165–185) highlighting the substitutions H176Y and T178R.

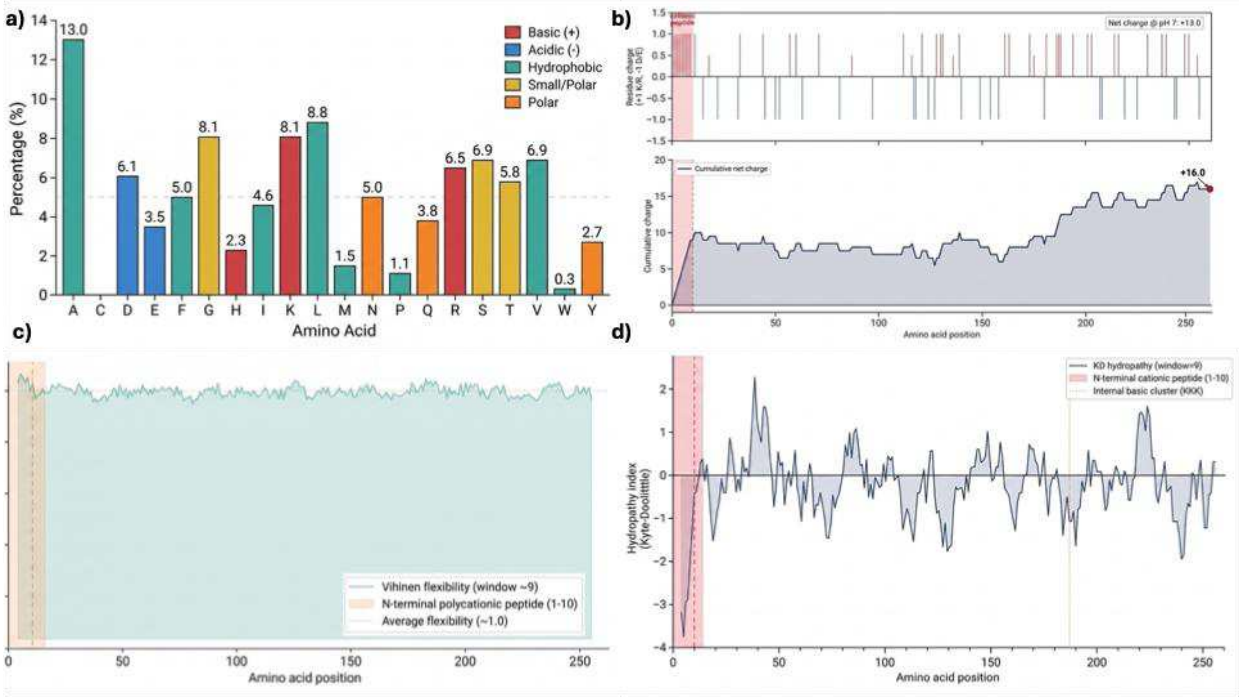
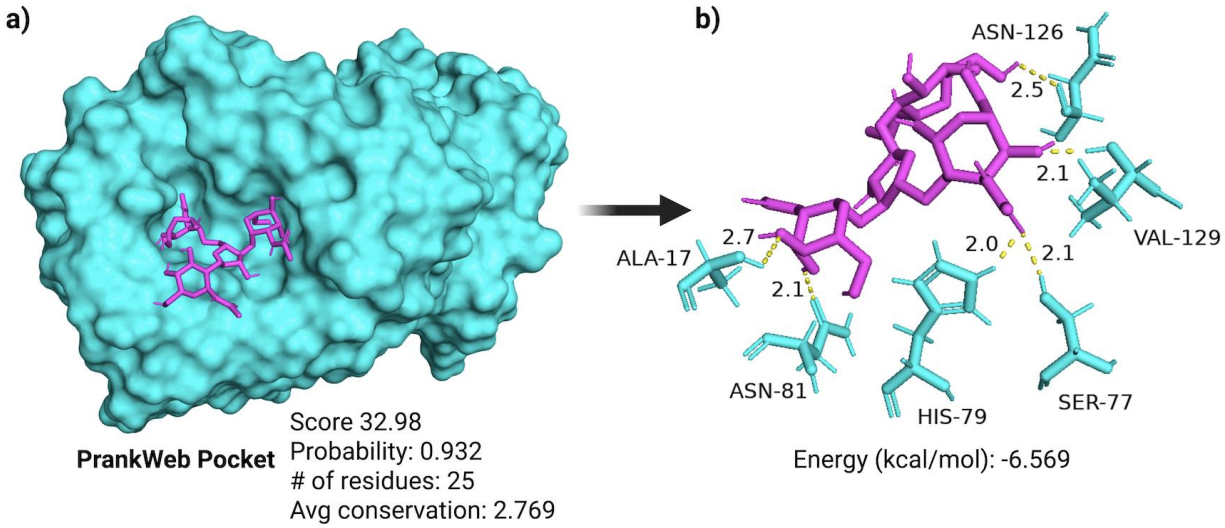


Figure 2. Physicochemical characterisation of ArtE2. (a) Amino-acid composition. (b) Charge distribution and cumulative net-charge profile; the N-terminal polycationic peptide is highlighted. (c) Vihinen flexibility profile (nine-residue window). (d) Kyte–Doolittle hydropathy profile.

373



374

375 **Figure 3.** Molecular docking of ArtE2 with the NAG–NAM dimer. (a) Surface representation showing
376 the ligand (magenta) bound in the top-ranked PrankWeb pocket. (b) Detailed interaction view with key
377 contacting residues and distances (Å). Vina score = −6.569 kcal mol^{-1}.

378

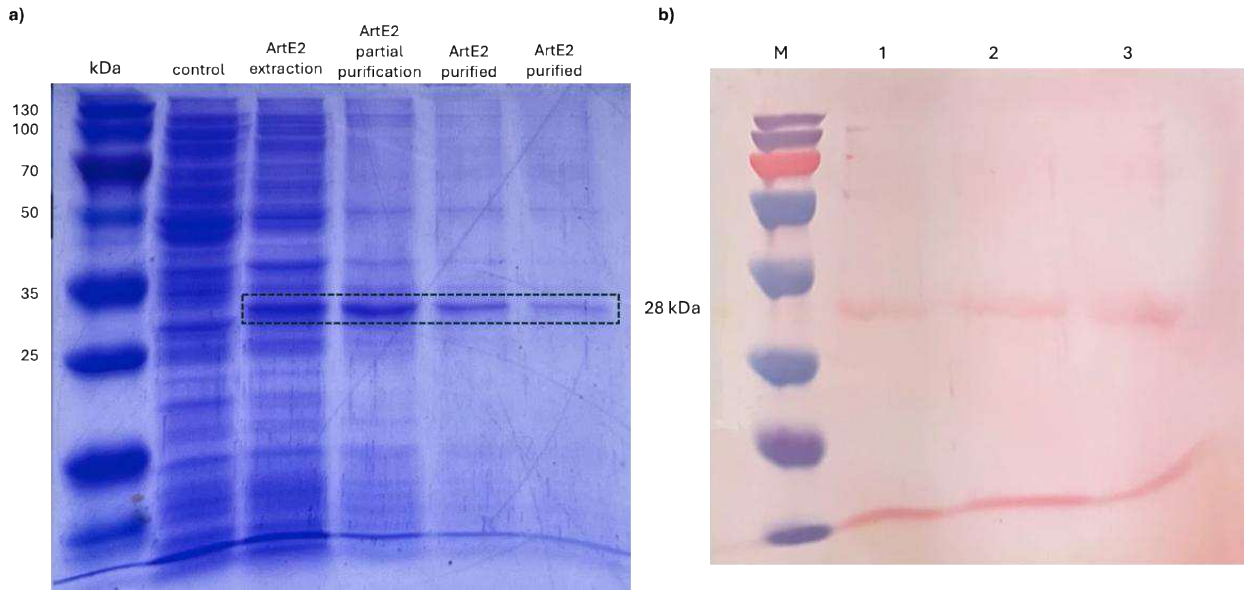


Figure 4. Expression and purification of recombinant ArtE2. (a) SDS-PAGE analysis of E. coli extract, ArtE2 extract, partially purified and purified fractions. The ~28 kDa band corresponding to ArtE2 is boxed. (b) Anti-His Western blot confirming the presence of the expected His-tagged protein.

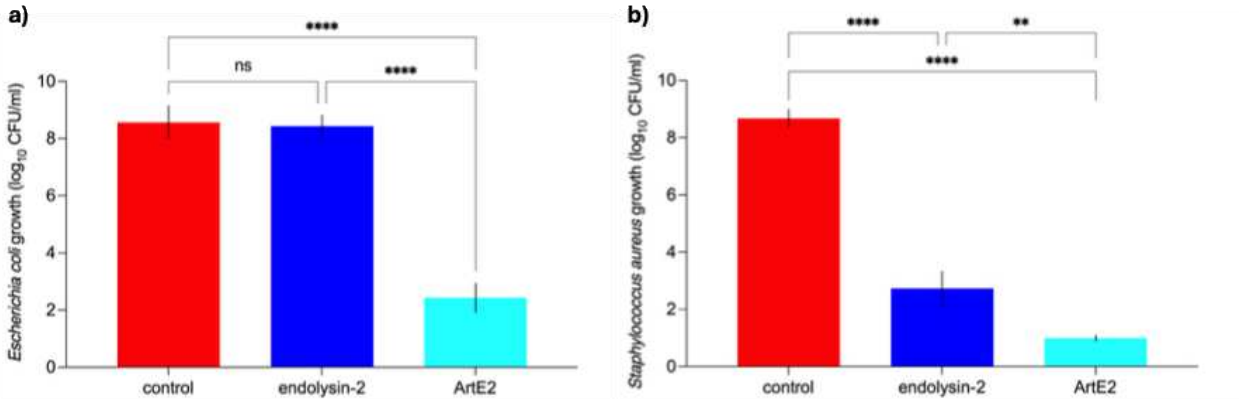


Figure 5. Antibacterial activity of native E2 and ArtE2 after 60 min exposure. (a) E. coli ATCC 25922. (b) S. aureus ATCC 25923. Data are mean ± SD of three independent biological replicates. **** $P < 0.0001$; ** $P < 0.01$; ns = not significant (one-way ANOVA).

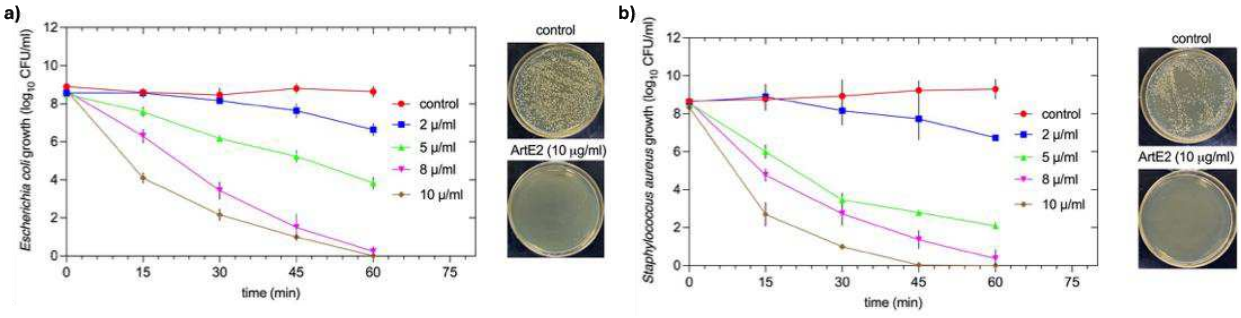


Figure 6. Concentration- and time-dependent antibacterial activity of ArtE2. (a) E. coli ATCC 25922. (b) S. aureus ATCC 25923. Viable counts (log_{10} CFU mL^{-1}) were determined at the indicated times after addition of ArtE2 (2–10 µg mL^{-1}). Representative plates at 60 min are shown.

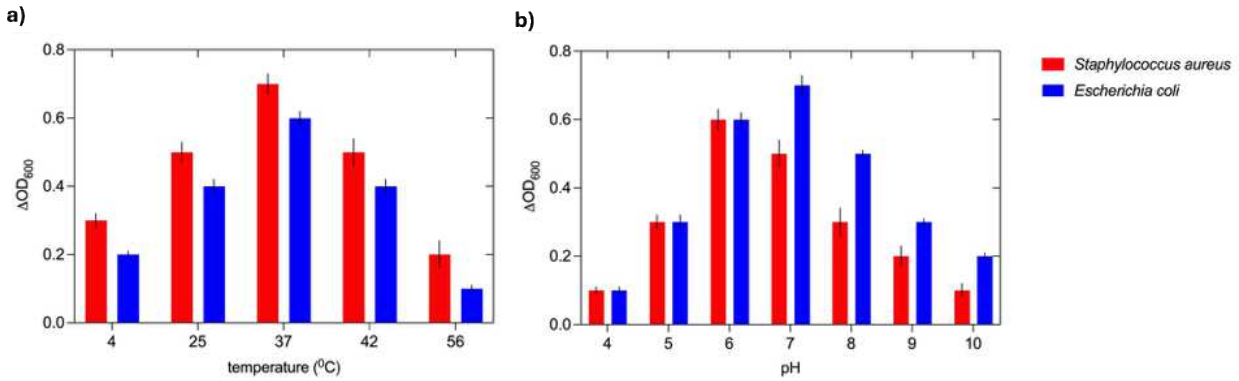


Figure 7. Effect of pre-incubation temperature and pH on residual ArtE2 activity. (a) Temperature (4–56 °C). (b) pH (4–10). Residual lytic activity was measured as ΔOD_{600} against S. aureus (red) and E. coli (blue). Data are mean ± SD of three independent replicates.

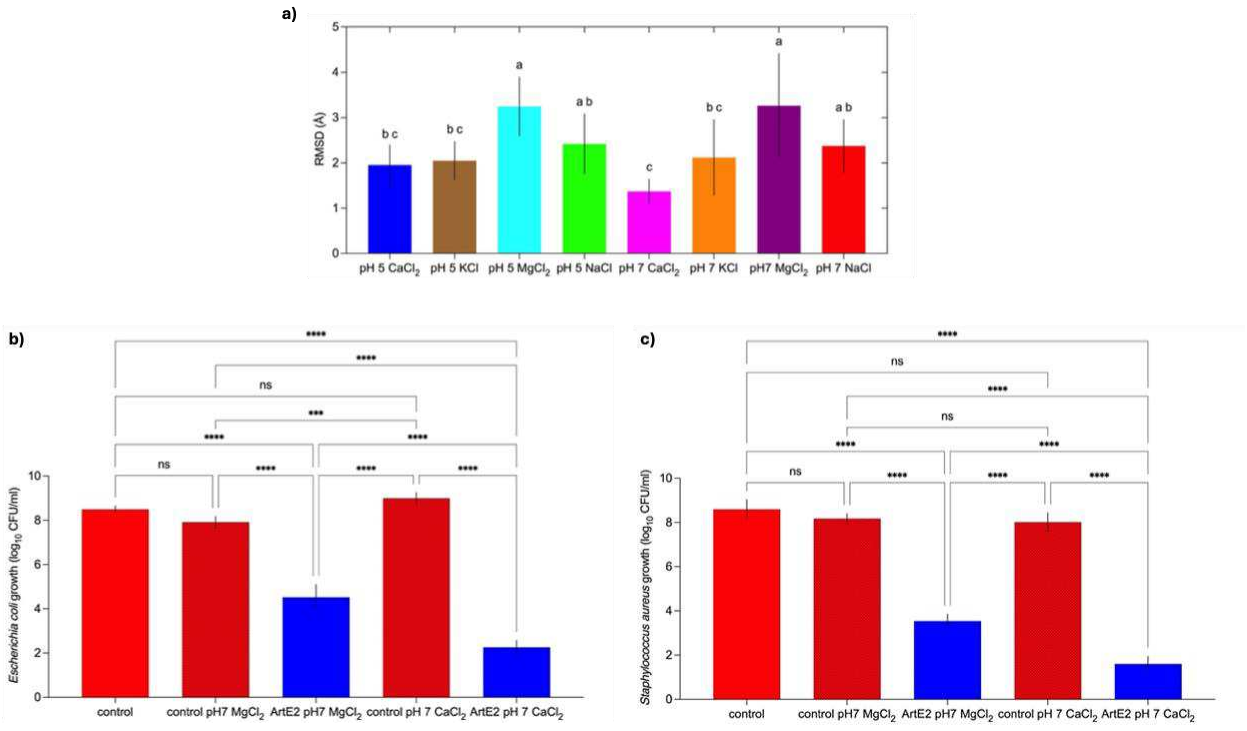


Figure 8. Molecular dynamics and corresponding antibacterial activity under selected ionic conditions. (a) Mean backbone RMSD of the ArtE2–NAG–NAM complex under different pH and salt conditions (three independent 1000-ns replicas). Letters indicate statistically distinct groups. (b, c) Antibacterial activity of ArtE2 at pH 7 in the presence of $MgCl_2$ or $CaCl_2$ against E. coli (b) and S. aureus (c).

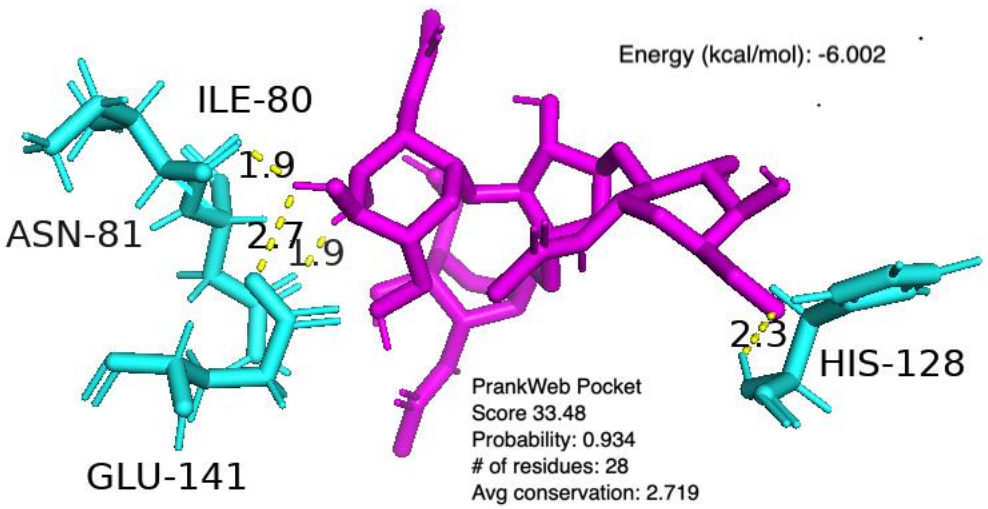


Figure S1. Molecular docking of native E2 with the NAG–NAM dimer (Vina score −6.002 kcal mol^{-1}).

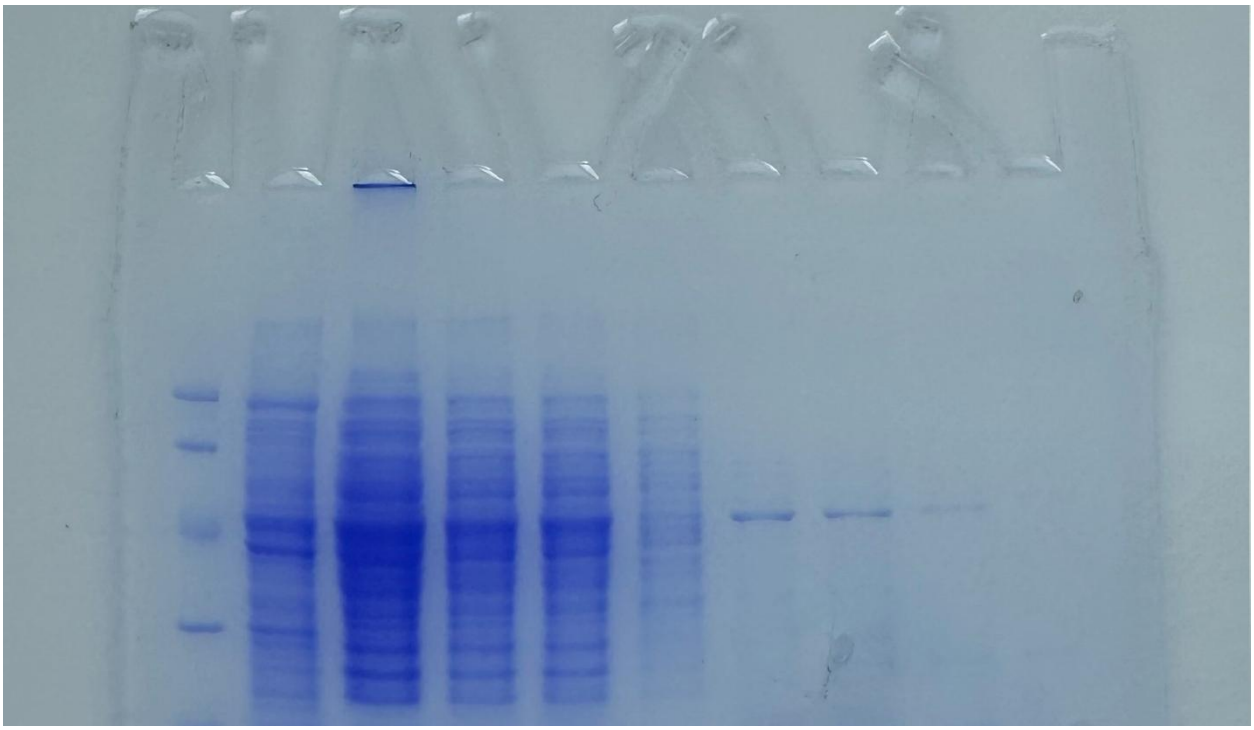


Figure S2. SDS-PAGE analysis of native E2 expression and purification.

Supplementary Table S1. DNA and amino acid sequences from artilysin ArtE2 and endolysin E2.

Artylisin (ArtE2)
DNA sequence
ATGAAACGCAAGAAACGTAAGAAACGCAAAGTAAAAATTTTCATCGATCCAGGTCATGGTGGCACGG ATAGCGGCGCAGCGGCTAACGGTCTGCTGGAAAAGAACATCACCCTGCAAATCGCGCTGTTCCTG CGCGACATGCTGATCAGCGAGTATGACGGTGTGTCCGTGCGTCTGTCCCGTTCCATTGACCAGTCT GTTACTCTGTCTCAACGTACGAACGCTGCCAACTCTTGGGGTGCGGATTACTTCGTGTCTATCCACAT CAACGCTGGTGGTGGTACGGGTTTCGAATCTTACGTTTACCCGGGTGTGAGCGCGCCTACGACCAC CTACCGTAACGCACTGCACGACGAGATCGTACGTTCCGTGGACTTTGCTGACCGTGGTAAGAAAAC CGCCAACTTCCACGTGCTGCGCGAAACCAGCATGTCCGCTATCCTGACCGAGAATGGCTTCATTGA CACGGTTGCTGATGCTAATAAACTGCGTAACGCCACCTTCCTGCAAGGTATCGCTCGTGCTCACGC GACTGGTCTGGAAAAAGCTCTGCAGCTGAAAAAGAAAGCGAGCAACCTGTACAAGGTTCAAGCCGG CGCATTCAAAGTGAAGGCGAACGCTGATGAACTGGCGGCTACGCTGCGTTCCAAAGGTTTCGAAGC GCTGGTAGTGCTGGACTCCGGTATGTACCGCGTTCAGGCTGGTGCTTTCCGTTCCAAACAGAACGC GGACGATCTGGTTGCGCGTCTGAAACAGGCGGGCCACGATGCGTTCGTGTTTCAGTAA
Amino acid sequence
MKRKKRKKRKVKIFIDPGHGGTDSGAAANGLLEKNITLQIALFLRDMLISEYDGVSVRLSRSIDQSVTLSQR TNAANSWGADYFVSIHINAGGGTGFESYVYPGVSAPTTTYRNALHDEIVRSVDFADRGKKTANFHVLRET SMSAILTENGFIDTVADANKLRNATFLQGIARAHATGLEKALQLKKKASNLYKVQAGAFKVKANADELAAT LRSKGFEALVVLDSGMYRVQAGAFRSKQNADDLVARLKQAGHDAFVFQ
Endolysin (E2)
DNA sequence
ATGGTGAAAATTTTTATTGATCCGGGCCATGGCGGCACCGATAGCGGCGCGGCGGCGAACGGCCT GCTGGAAAAAAACATTACCCTGCAGATTGCGCTGTTTCTGCGCGATATGCTGATTAGCGAATATGATG GCGTGAGCGTGCGCCTGAGCCGCAGCATTGATCAGAGCGTGACCCTGAGCCAGCGCACCAACG CGGCGAACAGCTGGGGCGCGGATTATTTTGTGAGCATTCATATTAACGCGGGCGGCGGCACCGGC TTTGAAAGCTATGTGTATCCGGGCGTGAGCGCGCCGACCACCACCTATCGCAACGCGCTGCATGA TGAAATTGTGCGCAGCGTGGATTTTGCGGATCGCGGCAAAAAAACCGCGAACTTTCATGTGCTGCG CGAAACCAGCATGAGCGCGATTCTGACCGAAAACGGCTTTATTGATACCGTGGCGGATGCGAACAA ACTGCGCAACGCGACCTTTCTGCAGGGCATTGCGCGCGCGTATGCGCGCGGCCTGGAAAAAGCG CTGCAGCTGAAAAAAAAAGCGAGCAACCTGTATAAAGTGCAGGCGGGCGCGTTTAAAGTGAAAGCG AACGCGGATGAACTGGCGGCGACCCTGCGCAGCAAAGGCTTTGAAGCGCTGGTGGTGCTGGATA GCGGCATGTATCGCGTGCAGGCGGGCGCGTTTCGCAGCAAACAGAACGCGGATGATCTGGTGGC GCGCCTGAAACAGGCGGGCCATGATGCGTTTGTGTTTCAG
Amino acid sequence
MVKIFIDPGHGGTDSGAAANGLLEKNITLQIALFLRDMLISEYDGVSVRLSRSIDQSVTLSQRTNAANSWG ADYFVSIHINAGGGTGFESYVYPGVSAPTTTYRNALHDEIVRSVDFADRGKKTANFHVLRETSMSAILTEN GFIDTVADANKLRNATFLQGIARAYARGLEKALQLKKKASNLYKVQAGAFKVKANADELAATLRSKGFEAL VVLDSGMYRVQAGAFRSKQNADDLVARLKQAGHDAFVFQ

References

1. Drew L. Are non-antibiotic drugs contributing to antimicrobial resistance? Nature. 2026;653:S12–S13.

2. Sati H, Carrara E, Savoldi A, Hansen P, Garlasco J, Campagnaro E, et al. The WHO Bacterial Priority Pathogens List 2024: a prioritisation study to guide research, development, and public health strategies against antimicrobial resistance. Lancet Infect Dis. 2025;25:1033–43.

3. Murray CJL, Ikuta KS, Sharara F, Swetschinski L, Aguilar GR, Gray A, et al. Global burden of bacterial antimicrobial resistance in 2019: a systematic analysis. Lancet. 2022;399:629–55.

4. Schmelcher M, Donovan DM, Loessner MJ. Bacteriophage endolysins as novel antimicrobials. Future Microbiol. 2012;7:1147–71.

5. Nelson DC, Schmelcher M, Rodriguez-Rubio L, Klumpp J, Pritchard DG, Dong S, et al. Endolysins as antimicrobials. Adv Virus Res. 2012;83:299–365.

6. Briers Y, Walmagh M, Van Puyenbroeck V, Cornelissen A, Cenens W, Aertsen A, et al. Engineered endolysin-based "Artilysins" to combat multidrug-resistant Gram-negative pathogens. mBio. 2014;5:e01379-14.

7. Briers Y, Walmagh M, Grymonprez B, Biebl M, Pirnay JP, Defraine V, et al. Art-175 is a highly efficient antibacterial against multidrug-resistant strains and persisters of Pseudomonas aeruginosa. Antimicrob Agents Chemother. 2014;58:3774–84.

8. Defraine V, Schuermans J, Grymonprez B, Govers SK, Aertsen A, Fauvart M, et al. Efficacy of Artilysin Art-175 against resistant and persistent Acinetobacter baumannii. Antimicrob Agents Chemother. 2016;60:3480–8.

9. Khan FM, Rasheed F, Yang Y, Liu B, Zhang R. Endolysins: a new antimicrobial agent against antimicrobial resistance—strategies and opportunities in overcoming the challenges of endolysins against Gram-negative bacteria. Front Pharmacol. 2024;15:1385261.

10. Gerstmans H, Criel B, Briers Y. Synthetic biology of modular endolysins. Biotechnol Adv. 2018;36:624–40.

11. Sisson HM, Jackson SA, Fagerlund RD, Warring SL, Fineran PC. Gram-negative endolysins: overcoming the outer membrane obstacle. Curr Opin Microbiol. 2024;78:102433.

12. Zheng T, Zhang C. Engineering strategies and challenges of endolysin as an antibacterial agent against Gram-negative bacteria. Microb Biotechnol. 2024;17:e14465.

13. Low LY, Yang C, Perego M, Osterman A, Liddington RC. Structure and lytic activity of a Bacillus anthracis prophage endolysin. J Biol Chem. 2005;280:35433–9.

14. Schuch R, Nelson D, Fischetti VA. A bacteriolytic agent that detects and kills Bacillus anthracis. Nature. 2002;418:884–9.

15. Portieles R, Ma X, Hu J, Xu Y, Xu H, Portal González N, et al. Integrated computational and experimental benchmarking of Bacillus phage endolysins reveals the relationship between peptidoglycan-fragment recognition descriptors and antibacterial performance. Sci Rep. 2026. https://doi.org/10.1038/s41598-026-57871-x.

16. Trott O, Olson AJ. AutoDock Vina: improving the speed and accuracy of docking with a new scoring function, efficient optimization, and multithreading. J Comput Chem. 2010;31:455–61.

17. Eberhardt J, Santos-Martins D, Tillack AF, Forli S. AutoDock Vina 1.2.0: new docking methods, expanded force field, and Python bindings. J Chem Inf Model. 2021;61:3891–8.

18. Antonova NP, Vasina DV, Rubalsky EO, Fursov MV, Savinova AS, Grigoriev IV, et al. Modulation of endolysin LysECD7 bactericidal activity by different peptide tag fusion. Biomolecules. 2020;10:440.

19. Nikaido H. Molecular basis of bacterial outer membrane permeability revisited. Microbiol Mol Biol Rev. 2003;67:593–656.

20. Wojciechowska M. Endolysins and membrane-active peptides: innovative engineering strategies against Gram-negative bacteria. Front Microbiol. 2025;16:1603380.

21. Aitken M, Abeysekera G, Billington C, Dobson RCJ. Recent advances in endolysin engineering. Antibiotics. 2025;14:1285.

22. Vasina DV, Antonova NP, Gushchin VA, Aleshkin AV, Fursov MV, Fursova AD, et al. Development of novel antimicrobials with engineered endolysin LysECD7-SMAP to combat Gram-negative bacterial infections. J Biomed Sci. 2024;31:75.

23. Cho J, Hong HW, Park K, Myung H, Yoon H. Unveiling the mechanism of bactericidal activity of a cecropin A-fused endolysin LNT113. Int J Biol Macromol. 2024;260:129493.

24. Lim J, Jang J, Myung H, Song M. Eradication of drug-resistant Acinetobacter baumannii by cell-penetrating peptide-fused endolysin. J Microbiol. 2022;60:859–66.

25. Jumper J, Evans R, Pritzel A, Green T, Figurnov M, Ronneberger O, et al. Highly accurate protein structure prediction with AlphaFold. Nature. 2021;596:583–9.

26. Abraham MJ, Murtola T, Schulz R, Páll S, Smith JC, Hess B, et al. GROMACS: high performance molecular simulations through multi-level parallelism from laptops to supercomputers. SoftwareX. 2015;1–2:19–25.

27. Huang J, Rauscher S, Nawrocki G, Ran T, Feig M, de Groot BL, et al. CHARMM36m: an improved force field for folded and intrinsically disordered proteins. Nat Methods. 2017;14:71–3.

Supplementary Files

This is a list of supplementary files associated with this preprint. Click to download.

- SupplementaryFigure.FulllengthoriginalunprocessedimagescorrespondingtoFigure4.pdf